

The role of acids in electrical conduction through ice

David E. Stillman,¹ Joseph A. MacGregor,² and Robert E. Grimm¹

Received 24 August 2012; revised 20 November 2012; accepted 1 December 2012.

[1] Electrical conduction through meteoric polar ice is controlled by soluble impurities that originate mostly from sea salt, biomass burning, and volcanic eruptions. The strongest conductivity response is to acids, yet the mechanism causing this response has been unclear. Here we elucidate conduction mechanisms in ice using broadband dielectric spectroscopy of meteoric polar ice cores. We find that conduction through polycrystalline polar ice is consistent with Jaccard theory for migration of charged protonic point defects through single ice crystals, except that bulk DC conduction is impeded by grain boundaries. Neither our observations nor modeling using Archie's Law support the hypothesis that grain-boundary networks of unfrozen acids cause significant electrolytic conduction. Common electrical logs of ice cores (by electrical conductivity measurement [ECM] or dielectric profiling [DEP]) and the attenuation of radio waves in ice sheets thus respond to protonic point defects only. This response implies that joint interpretation of electrical and chemical logs can determine impurity partitioning between the lattice and grain boundaries or inclusions. For example, in the Greenland Ice Core Project (GRIP) ice core from central Greenland, on average more than half of the available lattice-soluble impurities (H^+ , Cl^- , NH_4^+) create defects. Understanding this partitioning could help further resolve the nature of past changes in atmospheric chemistry.

Citation: Stillman, D. E., J. A. MacGregor, and R. E. Grimm (2013), The role of acids in electrical conduction through ice, *J. Geophys. Res.*, 118, doi:10.1029/2012JF002603.

1. Introduction

[2] Studies of ice in nature often rely on remote sensing using a broad portion of the electromagnetic spectrum, from direct current to optical frequencies. Detailed knowledge of the electrical properties of ice is therefore valuable for the study of diverse frozen environments. Understanding the direct current (DC; effectively $< \sim 10^{-1}$ Hz) and high-frequency (HF; $\sim 10^4$ – 10^8 Hz) electrical properties of meteoric polar ice is particularly important because these properties have been exploited extensively to study paleoclimate using electrical logs of ice cores [e.g., Taylor *et al.*, 1993; Wolff, 2000], the history and structure of the Greenland and Antarctic ice sheets using radar sounding [e.g., Dowdeswell and Evans, 2004], and ice-neutrino interactions [e.g., Barrella *et al.*, 2011].

[3] The electrical properties of laboratory-frozen ice have been studied extensively for more than 60 years [e.g., Auty and Cole, 1952; Camplin *et al.*, 1978; Johari and Whalley, 1981; Takei and Maeno, 1987; Grimm *et al.*, 2008; Stillman

et al., 2010, 2013]. Electrical conduction through laboratory-frozen single crystals is well described by the movement of charged protonic point defects formed by lattice-soluble impurities, a hypothesis originally developed by Jaccard [1959] (hereafter Jaccard theory; described in further detail in section 2). Following Jaccard theory, the conductivity of ice is frequency-, temperature-, and impurity-dependent. Conduction through naturally formed ice is perhaps inevitably more complex because it is generally polycrystalline, has a variable crystal orientation fabric, and contains trace concentrations of various impurities [e.g., Wolff *et al.*, 1997; Kulesa, 2007]. These impurities either substitute for or ionize H_2O molecules in the ice lattice (forming defects following Jaccard theory), are enclathrated, or remain in pore spaces (grain boundaries or inclusions) [e.g., Barnes and Wolff, 2004; Obbard and Baker, 2007].

[4] Of all the soluble impurities common in polar ice, acids produce the largest conductivity response per unit bulk concentration across a surprisingly large frequency range [Wolff *et al.*, 1997]. Studies of meteoric polar ice cores using near-DC electrical conductivity measurements (ECM) have shown that ECM varies nonlinearly with bulk acidity, but has no discernible relationship with other soluble impurities. Dielectric profiling (DEP; up to 300 kHz) logs of ice cores have shown that the HF conductivity of ice is most strongly proportional to bulk acidity but that it is also proportional to bulk concentrations of chloride (Cl^-) and ammonium (NH_4^+).

[5] Jaccard theory can explain the HF behavior of Cl^- and NH_4^+ , which create protonic point defects by producing Bjerrum L- and D-defects, respectively (hereafter simply

¹Department of Space Studies, Southwest Research Institute, Boulder, Colorado, USA.

²Institute for Geophysics, The University of Texas at Austin, Austin, Texas, USA.

Corresponding author: D. E. Stillman, Department of Space Studies, Southwest Research Institute, Boulder, Colorado, 80302, USA. (dstillman@boulder.swri.edu)

©2012. American Geophysical Union. All Rights Reserved. 2169-9003/13/2012JF002603

D- and L-defects) [Moore *et al.*, 1994a]. The mechanism by which acids increase both DC and HF electrical conduction through ice is less clear. Two mechanisms have been hypothesized to explain the role of acids in DC conduction [Wolff *et al.*, 1997]. The first mechanism is rooted in Jaccard theory: acid cations (H^+) produce ionic defects (H_3O^+) in the ice lattice, increasing intracrystalline conduction. This mechanism is supported by observations of an ECM response within large crystals of at least one polar ice core [Taylor *et al.*, 1997]. The second mechanism is electrolytic conduction of acidic liquids through grain-boundary networks [Wolff and Paren, 1984]. If such networks exist, they are likely liquid at terrestrial ice sheet temperatures ($>-60^\circ C$). This alternative mechanism is supported by observations of acid anions and associated elements at triple junctions [e.g., Mulvaney *et al.*, 1988; Barnes and Wolff, 2004] and veins [Fukazawa *et al.*, 1998], but those studies could not determine directly if acid cations were also present there. The strong HF response to acids has been suggested to be due to the large DC response to liquid triple junctions [Wolff *et al.*, 1997].

[6] To elucidate conduction mechanisms in polar ice, here we explore its electrical properties using broadband (10^{-2} – 10^6 Hz) dielectric spectroscopy of ice cores from both Greenland and Antarctica across a large temperature range ($-90^\circ C$ to $-5^\circ C$). Broadband measurements permit simultaneous characterization of both the DC and HF behavior of ice, so they are well suited to investigation of the dominant effect of acids upon its conductivity. We then reconsider the electrolytic conduction hypothesis for acids, analyze both our data and the response of ice core electrical logs (ECM, DEP) to acids in terms of Jaccard theory, and discuss the implications of our results for both radar sounding and studies of paleoclimate from electrical logs.

2. Jaccard Theory

[7] We first review Jaccard theory briefly, following Petrenko and Whitworth [1999] (their section 4.5). At its essence, Jaccard theory describes how polarization and conduction occur in ice crystals. The interdependence of these two processes arises from the nature of charge transfer through the ice lattice, which occurs by the flow of protons (H^+) due to migration of protonic point defects.

[8] Four types of protonic point defects are postulated, which are divided into two groups: ionic defects (H_3O^+ and OH^-) and L- and D-defects. Ionic defects are essentially ionized H_2O molecules. OH^- defects are believed to be uncommon in polar ice, but H^+ ions from dissociated acids can form extrinsic H_3O^+ defects. Bjerrum defects occur where a hydrogen bond has either no (L-defect) or two (D-defect) H^+ associated with it. Bjerrum defects are intrinsic in ice, i.e., they are always present, while both ionic and Bjerrum defects can be formed extrinsically by soluble impurities. Extrinsic Bjerrum defects are formed where an ion of similar covalent radius to O^{2-} but different charge substitutes for O^{2-} . In polar ice, the most common impurities capable of this substitution are Cl^- and NH_4^+ , which form extrinsic L- and D-defects, respectively. In the absence of extrinsic defects, intrinsic Bjerrum defects permit polarization in pure ice.

[9] The conductivity σ_i due to each defect type is the product of the defect's volumetric concentration n_i ,

temperature- and concentration-dependent mobility μ_i , and effective charge e_i :

$$\sigma_i = n_i \mu_i |e_i|. \quad (1)$$

[10] The subscript i denotes each type of defect, including intrinsic Bjerrum defects (in L and in D) and extrinsic ionic (H_3O^+ , and OH^-) and Bjerrum defects (ex L and ex D). These conductivities are summed by defect group (\pm : ionic; DL: Bjerrum) as

$$\sigma_{\pm} = \sigma_{H_3O^+} + \sigma_{OH^-}, \quad (2)$$

$$\sigma_{DL} = \sigma_{exD} + \sigma_{exL} + \sigma_{inL} + \sigma_{inD}. \quad (3)$$

[11] The contribution of these defects to the static (DC) conductivity of a single ice crystal (σ_s) is

$$\frac{e^2}{\sigma_s} = \frac{e_{\pm}^2}{\sigma_{\pm}} + \frac{e_{DL}^2}{\sigma_{DL}} \quad (4)$$

and the HF-limit conductivity σ_{∞} is simply the sum of the ionic and Bjerrum defect conductivities:

$$\sigma_{\infty} = \sigma_{\pm} + \sigma_{DL}. \quad (5)$$

[12] The Debye relaxation time τ , related to relaxation frequency as $f_r = 1/2\pi\tau$, is the mean time it takes for polarization to occur:

$$\frac{1}{\tau} = 1.8 \times 10^{-32} T \left(\frac{\sigma_{\pm}}{e_{\pm}^2} + \frac{\sigma_{DL}}{e_{DL}^2} \right), \quad (6)$$

where T is temperature. Finally, the dielectric susceptibility $\Delta\epsilon'$ describes the magnitude of the ice crystal's Debye relaxation and is related to τ as

$$\Delta\epsilon' = \frac{\sigma_{\infty} - \sigma_s}{\epsilon_0} \tau = \frac{(\sigma_{\pm}/e_{\pm} - \sigma_{DL}/e_{DL})^2}{1.8 \times 10^{-32} \epsilon_0 T (\sigma_{\pm}/e_{\pm}^2 + \sigma_{DL}/e_{DL}^2)^2}, \quad (7)$$

where ϵ_0 is the permittivity of the vacuum. Note that if the two terms in the numerator are equal, no relaxation is predicted.

[13] This notation and all other notation used are tabulated at the end of this paper. Values for the charge, defect mobility and activation energy of the defect mobility are given in Table 1. We assume that σ_{OH^-} and σ_{inD} are negligible because of the presumably negligible concentration of OH^- defects in meteoric polar ice and because of the low value of μ_{exD} , respectively [Stillman *et al.*, 2013]. The latter argument assumes that $\mu_{inD} \ll \mu_{inL}$ so that $\sigma_{inD} \ll \sigma_{inL}$.

[14] The frequency dependence of ice's conductivity arises from the migration of protonic point defects in an alternating electric field. In pure ice at $-20^\circ C$, this dielectric (Debye) relaxation typically peaks at $\sim 10^3$ Hz [e.g., Auty and Cole, 1952]. At frequencies below the Debye relaxation, conductivity approaches its DC (0 Hz) value; above this relaxation, between 10^4 and 10^8 Hz, conductivity plateaus at its HF limit. At both higher temperatures and defect/impurity concentrations, the relaxation peaks at a higher frequency, due to increasing defect mobility and concentration, respectively. Higher relaxation frequencies increase HF conductivity.

Table 1. Parameter Values Used for Jaccard Theory Modeling

Defect type	e_i (1.609×10^{-19} C)	μ_i at -20°C (10^{-8} m ² V ⁻¹ s ⁻¹)	E_i^a (eV)
H ₃ O ⁺	0.62	10	0.21
in L	0.38	2	0.58
ex L	0.38	2	0.23
ex D	0.38	0.16 ^b	0.23 ^b

^aActivation energies are used to correct values to -15°C (e.g., equation (2)), which is the temperature of the empirical chemistry—DEP relationship for GRIP (equation (3)). All values are from *Petrenko and Whitworth* [1999] (their Table 6.4, p. 154) unless otherwise noted. Uncertainties are of the order of 0.01e for the defect charges, 50% for mobilities, and less than 25% for activation energies.

^bData from *Stillman et al.* [2013].

[15] Jaccard theory in its classic form is valid for single ice crystals only. Hence, it does not consider the possible electrical effect of any impurities excluded to pore spaces (grain boundaries and/or inclusions), which commonly occurs in polar ice.

3. Samples and Methods

[16] Based on existing chemistry logs, we selected 26 samples from six different polar ice cores drilled within the Greenland and Antarctic ice sheets (Table 2). These samples were provided by the U.S. National Ice Core Laboratory, which stored them at -35°C . The samples were selected from

a range of climatic and glaciological conditions, including ice deposited during both volcanic eruptions and conditions typical of interglacial and glacial periods, which resulted in a range of chemical compositions. All samples were meteoric, and most (19/26) were recovered from deeper than 100 m below the ice sheet surface, so their density is close to that of pure ice.

[17] The ice core samples (9–31 cm³) were microtomed to produce two smooth parallel surfaces and then loaded into a three-electrode parallel plate capacitor. This capacitor was composed of a fixed unguarded electrode (55 mm diameter), a guarded electrode whose diameter (10–30 mm) varied depending on sample size, and a grounded guard electrode that fringed the difference in diameter between the guarded and unguarded electrodes. The complex impedance of the ice-filled capacitor was measured as a function of frequency and temperature using a Solartron 1260A impedance analyzer and a Solartron 1296A dielectric interface. The high input impedance (10^{14} Ω) enables measurement of conductivities as low as 10^{-12} S m⁻¹. Measurement temperatures varied between -90°C and -5°C , but were typically between -85°C and -40°C at 5 K intervals. Measurements within this temperature range are easiest to interpret using Cole—Cole modeling (discussed below). See *Grimm et al.* [2008] for additional details on the measurement apparatus. We converted the measured complex impedance into complex permittivity using the capacitor geometry.

[18] Figure 1 shows examples of measured complex permittivity spectra from the six different ice cores at a single temperature and for a single sample across a temperature

Table 2. Depth and Lattice-Soluble Impurity Concentrations of Our Ice Core Samples Estimated From Depth-Adjacent Chemistry Logs

Ice core ^a	Depth (m)	[H ⁺] (μM)	[Cl ⁻] (μM)	[NH ₄ ⁺] (μM)	Notes
GISP2	505.250	2.2	0.3	0.2	Holocene origin
GISP2	1404.000	0.3	0.2	1.1	High [NH ₄ ⁺]
GISP2 ^b	1406.300	0.0	0.3	5.9	Very high [NH ₄ ⁺]
GISP2	1709.960	0.0	2.5	1.7	High [NH ₄ ⁺]
GISP2	1791.960	0.2	0.9	0.2	
GISP2	2549.860	0.0	2.1	0.1	High [SO ₄ ²⁻] (1.7 μM)
Newall Glacier	51.000	2.5	4.6	N/A	Average impurities
Newall Glacier ^b	80.250	1.4	3.8	N/A	Average impurities
Newall Glacier	102.290	0.0	4.1	N/A	
Newall Glacier	120.005	0.0	5.3	N/A	
Newall Glacier	133.010	0.0	10.3	N/A	High [SO ₄ ²⁻] (16.7 μM)
Siple Dome ^b	54.950	0.6	13.8	N/A	High [Cl ⁻]
Siple Dome	185.350	3.1	7.5	N/A	High [H ⁺]
Siple Dome	558.752	1.4	2.7	N/A	Low impurities
Siple Dome	719.240	0.3	4.8	N/A	
South Pole	51.100	2.6	0.7	0.1	Average impurities
South Pole	69.935	2.2	0.6	0.2	High [H ⁺]
South Pole	89.010	3.5	1.3	0.1	High [SO ₄ ²⁻] (1.3 μM)
South Pole ^b	92.030	0.0	0.4	2.3	High [NH ₄ ⁺]
South Pole	138.680	0.9	1.4	0.6	
Taylor Dome ^b	102.110	1.6	1.2	0.6	Average impurities
Taylor Dome	374.890	0.1	4.6	0.0	High impurities
Taylor Dome	543.970	0.9	1.1	0.1	Average impurities
Vostok	429.120	0.0	7.0	0.1	High impurities
Vostok ^b	2044.080	0.0	4.6	0.1	High dust concentration
Vostok ^c	3477.755	1.4	2.3	0.1	Basal ice

^aData sources for [H⁺], [Cl⁻], and [NH₄⁺] are as follows. GISP2: *Yang et al.* [1997]; Newall Glacier: *Mayewski et al.* [1995a]; Siple Dome: *MacGregor et al.* [2007]; South Pole: *Cole-Dai* [2004]; Taylor Dome: *Mayewski et al.* [1995b]; Vostok: *Petit et al.* [1999]. Qualitative descriptions of impurity content are given within the context of all the available chemistry data for that ice core.

^bThe complex permittivity spectrum of the sample at this depth is shown as representative of that ice core in Figures 1a–c.

^cThis Vostok sample is from a basal ice unit that contains increased concentrations of glacial flour but its ice is meteoric in origin [*Souchez et al.*, 2002].

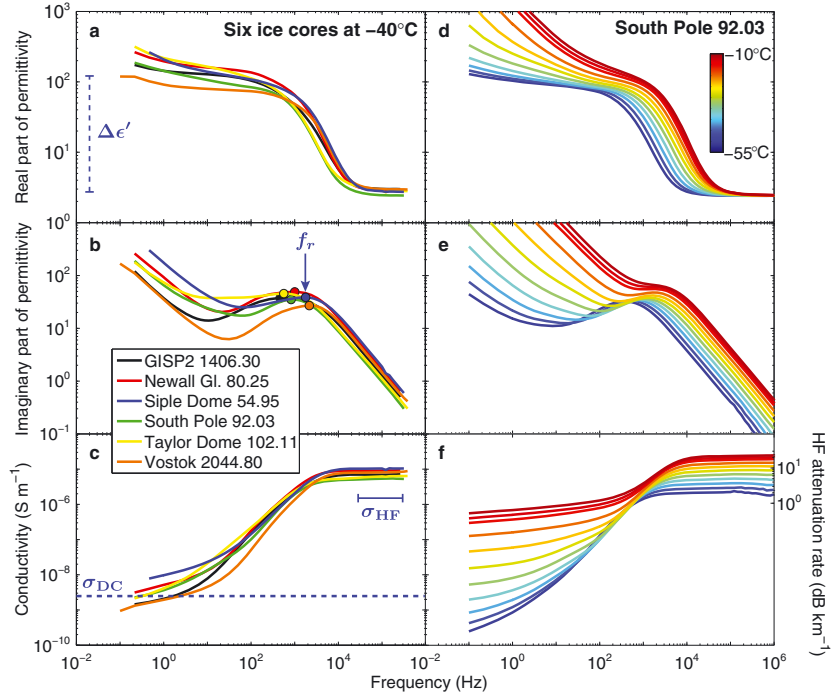


Figure 1. (a–c) Complex permittivity of six ice core samples at -40°C (depths in meters given in legend). These data reveal the broadband character of the well-known dielectric variability of meteoric ice and are typical of the range of complex permittivity spectra we measured. The key dielectric properties of the representative Siple Dome sample (blue) are highlighted: DC conductivity (σ_{DC}), HF conductivity (σ_{∞}), dielectric susceptibility ($\Delta\epsilon'$), and primary Debye relaxation frequency (f_r). All values were determined using Cole–Cole modeling (equation (8)) except for σ_{∞} , which was measured directly. (d–f) The temperature dependence of the complex permittivity of a sample from the South Pole, whose temperature-dependent behavior is typical of the ice cores we examined (Figure 2). For Figure 1f, the HF attenuation rate equivalent to the HF conductivity is given on the right-hand y-axis [e.g., *MacGregor et al.*, 2007].

range. We then modeled the measured spectrum using multiple Cole–Cole relaxations and DC conductivity at each temperature [e.g., *Grimm et al.*, 2008; *Stillman et al.*, 2010]:

$$\epsilon^* = \epsilon' - i\epsilon'' = \epsilon_{\infty} + \sum_{j=1}^N \frac{\Delta\epsilon'_j}{1 + (i\omega\tau_j)^{1-\alpha_j}} - \frac{i\sigma_{\text{DC}}}{\epsilon_0\omega}, \quad (8)$$

where ϵ^* is the complex permittivity, ϵ' and ϵ'' are its real and imaginary parts, respectively, ϵ_{∞} is the HF permittivity, N is the total number of observed dielectric relaxations, α is the Cole–Cole distribution parameter ($\alpha=0$ for a Debye relaxation), $i = \sqrt{-1}$, σ_{DC} is the DC conductivity, and ω is the angular frequency. Where σ_{DC} does not clearly asymptote with frequency, we infer σ_{DC} from our band-limited complex permittivity data using equation (8).

[19] The temperature dependence of σ_{DC} is fit using a generalized Boltzmann model:

$$\sigma_{\text{DC}} = \sigma_{\text{DC}}^0 \exp\left[\frac{E_{\text{DC}}}{k} \left(\frac{1}{T_0} - \frac{1}{T}\right)\right], \quad (9)$$

where σ_{DC}^0 is the DC conductivity at a reference temperature T_0 , E_{DC} is its activation energy, and k is the Boltzmann constant [e.g., *Stillman et al.*, 2010].

[20] Uncertainties estimated from repeat measurements are 5% for the real part of the permittivity and 10% for the

imaginary part (conductivity). The 95% confidence bounds for the Cole–Cole parameters were estimated using $\Delta\chi^2$ distributions that accounted for these uncertainties. Reported HF-limit conductivities (σ_{∞}) are the mean value over the frequency range where conductivity plateaus (typically 10^4 – 10^5 Hz).

[21] We attempted to measure the meltwater chemistry of our samples after completing our dielectric measurements, but the column used to filter the meltwater prior to measurement by ion chromatography was contaminated by earlier samples that were significantly more impure than melted meteoric ice. Instead, we estimated the bulk chemistry of our ice core samples from the closest available depth in available ion chromatography logs for each ice core. Bulk acid concentrations ($[\text{H}^+]$ or acidity) were calculated using the charge balance of measured soluble ions following *MacGregor et al.* [2007].

4. Results

4.1. DC Conductivity

[22] Only 20 of our 26 samples have detectable values of σ_{DC} . For some samples with detectable σ_{DC} , at lower temperatures ($<-40^{\circ}\text{C}$) we were able to determine the upper limit of its 95% confidence bound only (Figure 2). The

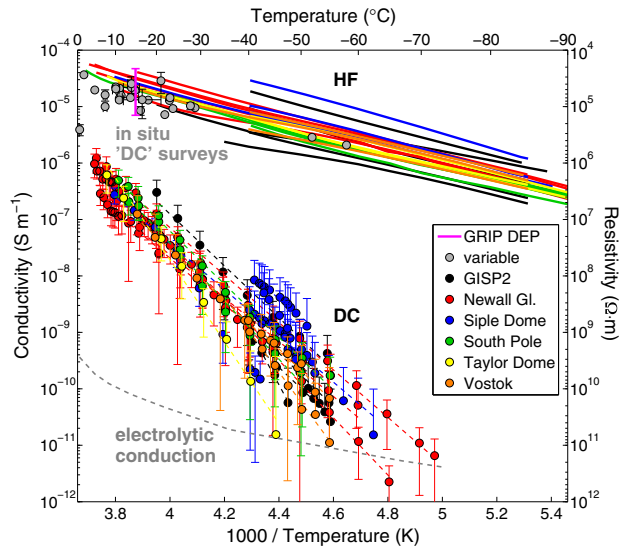


Figure 2. DC and HF conductivity of all meteoric ice cores we measured, excepting the sample shown separately in Figure 4. Colored dashed lines are the regressions of modeled DC conductivity of each sample for the temperature range over which it was measured. The entire range of DEP σ_{∞} values from the GRIP ice core (close to GISP2) is shown in magenta [Wolff *et al.*, 1995]. Data from georesistivity surveys of various locations on polar ice sheets and ice caps [Reynolds and Paren, 1984; Shabtaie and Bentley, 1995] were assumed to represent the DC conductivity of polar ice. The modeled DC conductivity due to electrolytic grain-boundary conduction is calculated using equation (12).

typical range of σ_{DC} for these samples at a given temperature is an order of magnitude, although this range approached two orders of magnitude at lower temperatures, where σ_{DC} is more difficult to constrain. The mean value of E_{DC} is 0.98 ± 0.25 eV, calculated using linear regressions in log space for each sample with detectable σ_{DC} .

[23] At high temperatures ($> -30^{\circ}\text{C}$), σ_{DC} for our ice-core samples is generally 1–2 orders of magnitude smaller than most previously reported values for polar ice, as measured by in situ DC georesistivity surveys [Reynolds and Paren, 1980, 1984] (Figure 2). This discrepancy is even larger at lower temperatures ($< -50^{\circ}\text{C}$), when compared to measurements from Dome C, East Antarctica [Shabtaie and Bentley, 1995].

[24] There are few previous laboratory-measured σ_{DC} values for polar ice with which to compare our data. Reynolds and Paren [1984] inferred a range of 9–12 $\mu\text{S m}^{-1}$ at -20°C for polar ice from laboratory measurements made by Fitzgerald and Paren [1975] and Paren [1973]. However, the low-frequency limit of those measurements was 60 Hz, and their reported conductivity spectra did not clearly reach the DC limit [e.g., Figure 1 in Fitzgerald and Paren, 1975]. Reynolds and Paren [1984] reported that $\sigma_{DC} = 16 \mu\text{S m}^{-1}$ at -7°C for the Byrd Station (West Antarctica) samples measured by Fitzgerald and Paren [1975]. However, at 60 Hz those data clearly show that their measured conductivity is $2 \mu\text{S m}^{-1}$ at -7°C and that it is still decreasing with decreasing frequency, i.e., they had not reached the DC limit,

which typically occurs below 10 Hz (e.g., Figures 1c and 1f). This observation indicates that $\sigma_{DC} < 2 \mu\text{S m}^{-1}$ at -7°C for those samples, in closer agreement with our data. It is also not clear that Reynolds and Paren [1984] inferred σ_{DC} from equation (8) rather than simply assuming that σ_{DC} was equal to the conductivity at the lowest measured frequency. We therefore discard their inferred σ_{DC} values. Separately, Moore *et al.* [1992a] presented DEP spectra for four meteoric ice samples from Dolleman Island (Antarctic Peninsula) that show that ice conductivity at 20 Hz is less than 10^{-8}S m^{-1} at -22°C , which is lower than our observed range at that temperature. However, the DEP apparatus could not measure σ_{DC} directly because of the air gap and electrically insulating polythene sleeve between its capacitor and the ice core.

[25] Three previous studies determined σ_{DC} for polar firm using methods similar to ours. Kopp [1962] measured five samples from 10 to 50 m in depth and reported $\sigma_{DC} \sim 7 \times 10^{-9} \text{S m}^{-1}$ at -10°C and $E_{DC} = 0.82$ eV. Maeno [1978] reported σ_{DC} values between 10^{-10} and 10^{-7}S m^{-1} at -10°C and $E_{DC} = 0.40$ eV for samples shallower than 55 m, while deeper samples had σ_{DC} between 10^{-8} and 10^{-5}S m^{-1} and $E_{DC} = 1.36$ eV. The lower density of firm should render it less conductive than ice [e.g., Barnes *et al.*, 2002], yet several of these measurements of σ_{DC} are similar to ours. Unfortunately, Maeno [1978] does not show or further discuss reported samples with high σ_{DC} values. Reynolds [1985] measured firm and ice from the top 8 m at four different locations in the Antarctic Peninsula and reported σ_{DC} values 3 orders of magnitude lower than the georesistivity surveys reported by Reynolds and Paren [1984] (Figure 2). This difference in conductivity from the laboratory to the georesistivity surveys was attributed to poor ohmic contact between the electrodes and the ice. While free charges cannot efficiently transfer between ice and metallic electrodes, rather than lowering σ_{DC} , poor ohmic contact allows charges to build up at the ice-electrode interface, inducing an electrode polarization. This effect is visible in Figure 1d as the sharp increase in ϵ' at low frequencies, and it can prevent measured conductivity from reaching its DC limit (Figure 1f). However, electrode polarization is incapable of lowering conductivity 3 orders of magnitude. We modeled this electrode polarization using equation (8) to separate its effect from σ_{DC} , and it is the primary source of uncertainty in our measurements of σ_{DC} (confidence bounds in Figure 2). Overall, previous σ_{DC} measurements of polar firm are more consistent with our measurements in terms of both magnitude and activation energy than those inferred from georesistivity surveys or laboratory measurements of polar ice.

[26] There is no clear relationship between bulk σ_{DC} and acidity (Figure 3), contrary to the well-established nonlinear response of ECM to acidity [Wolff *et al.*, 1997]. While the temperature dependence of each sample varied, we do not observe any discontinuity or change in temperature dependence in σ_{DC} when warming samples across the eutectic temperatures of the three acids common in meteoric ice (H_2SO_4 , HCl, HNO_3 ; -67°C , -85°C , and -41°C , respectively). This observation suggests that a single conduction mechanism dominates DC behavior generally.

[27] Only one sample (Newall Glacier 80.27 m) shows evidence of a eutectic-related change in conductivity, but between -50°C and -60°C instead of the eutectic temperature of the one of the common acids (Figure 4). The large (> 1)

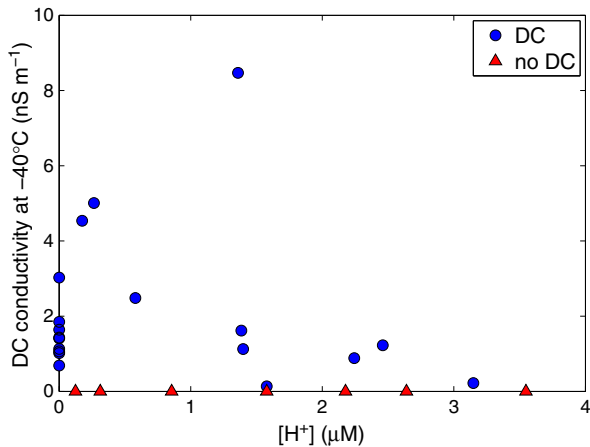


Figure 3. Relationship between bulk acidity ($[H^+]_{bulk}$) and DC conductivity. Blue circles represent samples where non-negligible DC conductivity was observed, and red triangles represent samples where none was observed. The poor correlation between these two quantities suggests that $[H^+]_{bulk}$ does not control DC conductivity; we attribute this variability to the grain boundaries present in polycrystalline polar ice (sections 5.2 and 6.2).

increase in ϵ_∞ suggests sudden melting of $CaCl_2$, whose eutectic temperature ($-51^\circ C$) lies within this temperature range. The strong low-frequency Maxwell–Wagner dielectric relaxation at ~ 4 Hz and the lack of a low-frequency conductivity limit suggest that any liquid brine that was formed is not interconnected throughout the sample but instead is restricted to inclusions that are likely located at triple junctions. Indeed, $CaCl_2$ has been found at grain boundaries in the Vostok ice core [Obbard and Baker, 2007]. Previous observations of laboratory-frozen doped ice suggest that these brine “pockets” become interconnected when their bulk concentration is greater than 3 mM [Grimm et al., 2008]. This concentration is 3 orders of magnitude higher than the typical background concentration of soluble impurities in polar ice [e.g., Legrand and Mayewski, 1997], suggesting the presence of $CaCl_2$ -rich inclusions. However, in the absence of additional measurements of the bulk impurity concentrations of this sample, we cannot further evaluate this eutectic behavior.

4.2. HF Conductivity

[28] Our measured σ_∞ range (~ 10 – $40 \mu S m^{-1}$ at $-20^\circ C$) matches the range of the georesistivity surveys and is also consistent with the σ_∞ range measured by DEP at $-15^\circ C$ [Moore et al., 1992a; Wolff et al., 1995, 1997] (Figure 2). If those georesistivity surveys had measured σ_{DC} accurately, then the small difference between their values and the well-established range of σ_∞ for meteoric ice would imply that there is no significant dielectric relaxation in meteoric ice. However, we consistently observe a strong ($\Delta\epsilon' > 100$) bulk dielectric relaxation in polar ice (e.g., Figure 1), as have others [e.g., Fitzgerald and Paren, 1975; Moore et al., 1992a].

[29] Our measured σ_∞ range can also be compared with two different empirical models of σ_∞ that predict its value from bulk chemistry and temperature [Wolff et al., 1997; MacGregor et al., 2007] (Figure 5). Bulk chemistry data

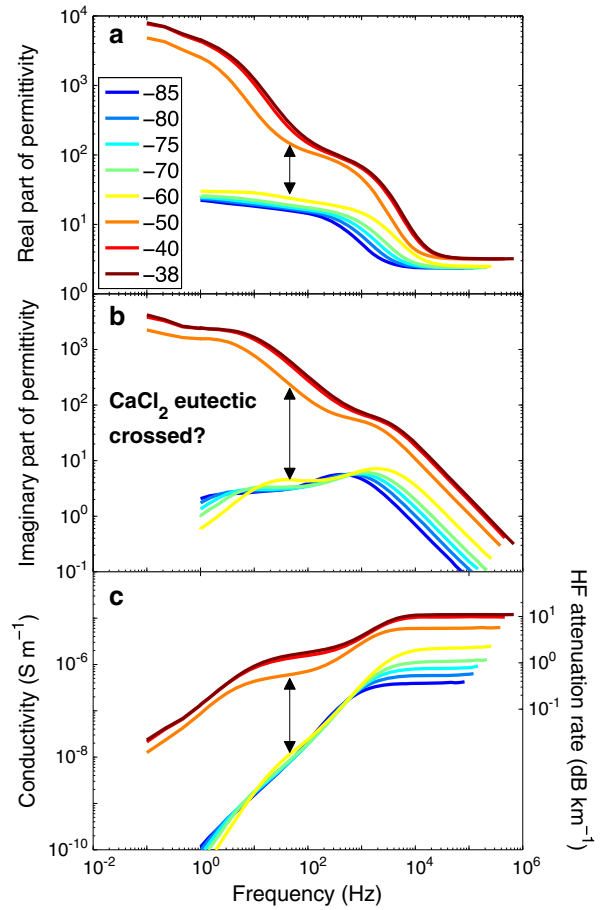


Figure 4. (a–c) Complex permittivity of a Newall Glacier sample (80.27 m depth) between $-85^\circ C$ and $-38^\circ C$, which is the only ice core sample we measured that displayed possible eutectic behavior. This sample is not shown in Figure 2. It is close in depth to another Newall Glacier sample (80.25 m) that is shown in Figure 2 but that did not display this behavior. Measurement temperature in degrees Celsius is given in legend in Figure 4a. As in Figure 1f, the HF attenuation rate equivalent to HF conductivity is given on the right-hand y-axis.

are unavailable for the samples we measured, so we modeled σ_∞ for our samples using the soluble chemistry of depth-adjacent melted samples (Table 2). For the Greenland Ice Core Project (GRIP) ice core in central Greenland, this relationship is [Wolff et al., 1997]

$$\sigma_\infty = 9 + 4[H^+] + 1[NH_4^+] + 0.55[Cl^-], \quad (10)$$

where σ_∞ is in units of $\mu S m^{-1}$ and the impurity concentrations are in units of μM . We then adjusted σ_∞ from $-15^\circ C$ to $-40^\circ C$ using a Boltzmann model (e.g., equation (9)) and the appropriate activation energy for each component (Table 1). We chose $-40^\circ C$ because it is the highest temperature at which all our samples were measured. The model presented by MacGregor et al. [2007] is similar but specifies different activation energies for each conductivity contribution and ignores the conductivity contribution of NH_4^+ .

[30] The correlation between measured and modeled σ_∞ is poor ($r < 0.40$ for both empirical models), which is likely

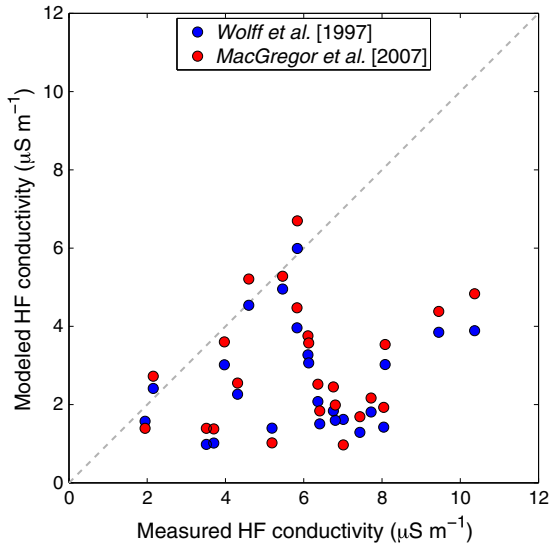


Figure 5. Measured and modeled HF conductivity of ice core samples at -40°C . Modeled HF conductivity is calculated using the soluble chemistry of depth-adjacent melted samples (Table 2) and existing empirical HF conductivity models [Wolff *et al.*, 1997; MacGregor *et al.*, 2007]. Two outlier samples from GISP2 (1404.00 m) and Siple Dome (185.35 m) are not shown, as their measured σ_{∞} values are ~ 5 times larger than the modeled values, likely due to anomalously high NH_4^+ and H^+ concentrations, respectively (Table 2).

due to the large variability of ice core chemistry with depth and the unavailability of direct chemistry data for our samples. The empirical models generally underestimate measured σ_{∞} , suggesting that their temperature dependence (activation energies) may be too high. However, the discrepancy between measured and modeled σ_{∞} is an order of magnitude less than that between our inferred σ_{DC} values and those reported by georesistivity surveys.

5. Conduction Mechanisms

[31] A comparison of our measurements of σ_{DC} and σ_{∞} of polar ice to the most reliable published values confirms that we measured both quantities accurately. This comparison suggests that the σ_{DC} values inferred from georesistivity surveys are inconsistent with our and virtually all other laboratory measurements of σ_{DC} . Critically, the electrolytic conduction hypothesis for DC conduction by acids was based on a subset of the same georesistivity survey data discussed above [Wolff and Paren, 1984]. Barnes and Wolff [2004] found significant heterogeneity in the distribution of soluble impurities in polar ice samples with low bulk impurity concentrations. They concluded that this heterogeneity implies that acids are unlikely to form vertically connected acid networks in large portions of an ice sheet, an important assumption underlying the electrolytic conduction hypothesis. However, Srikanta Dani *et al.* [2012] suggested recently that the size of impurity-rich veins is non-negligible throughout the vertical extent of an ice sheet. The combination of these results and ours warrants reconsideration of hypothesized conduction mechanisms in polar ice, which we undertake below.

5.1. Electrolytic Conduction due to Acid-Filled Triple Junctions

[32] Mulvaney *et al.* [1988] discovered sulfur at triple junctions in an ice core sample from the Antarctic Peninsula. They argued that 40–100% of the sulfuric acid (H_2SO_4) in their sample resides at triple junctions, and that at those locations it must be sufficiently concentrated such that the acid is liquid above its eutectic temperature. This observation supported an earlier quantitative model of electrolytic conduction by acids at grain boundaries that assumed a linear relationship between DC conductivity and the liquid fraction of ice [Wolff and Paren, 1984]:

$$\sigma_{\text{DC}} = \frac{1}{3} \sigma_{\text{liq}} \phi, \quad (11)$$

where σ_{liq} is the DC conductivity of the liquid matrix and ϕ is the bulk porosity, which is equal to the liquid fraction if pores are assumed to be liquid-filled. This model treats ice as a simple parallel circuit, maximizing conduction through the bulk sample. No consolidated geologic materials are known to behave in this way [Keller, 1982].

[33] Alternatively, Archie’s Law is a general empirical DC conduction model for materials composed of poorly conducting grains with both variable welding and geometry surrounded by a conducting liquid [e.g., Archie, 1942]:

$$\sigma_{\text{DC}} = S^{\beta} \sigma_{\text{liq}} \phi^m, \quad (12)$$

where S is the relative saturation (fractional liquid saturation of the pore volume), β is the saturation exponent, and m is the cementation exponent of the material. Equation (12) reduces to equation (11) if $S^{\beta} = 1/3$ and $m = 1$. Archie’s Law accounts for the matrix tortuosity inherent in consolidated geologic materials, which limits intergranular conduction, and it is used widely in hydrocarbon exploration to interpret electrical logs from boreholes [e.g., Torres-Verdin *et al.*, 2006].

[34] Assuming that ice is composed of semiregular truncated octahedra, Nye and Frank [1973] calculated its porosity to be $\phi = 3\pi(w/D)^2$, where w is the triple junction radius and D is the grain diameter. Using this geometric model, Grimm *et al.* [2008] found that $m = 2.1$ for salt-doped laboratory-frozen ices that clearly displayed electrolytic conduction due to large initial solution concentrations (> 3 mM). We assume that acidic liquid always fills the triple junctions, so that $S = 1$ and β can be ignored. The assumed size and concentration of the triple junctions are valid at or above the eutectic temperature of H_2SO_4 . Above this temperature, the acid concentration is diluted as it melts and increases the size of the triple junctions, so that both ϕ and σ_{liq} are temperature- and concentration-dependent. σ_{liq} has an Arrhenius-form temperature dependence with an activation energy of 0.11 eV at a constant concentration [Lide, 2008].

[35] We modeled σ_{DC} for an ice sample based on Mulvaney *et al.*’s [1988] inferred values of triple-junction cross-sectional area ($0.5 \mu\text{m}^2$) and H_2SO_4 concentration (the eutectic composition, 4.9 M). Other stronger acids (e.g., HCl) are also present in meteoric ice [Wolff *et al.*, 1997], but their electrolytic conductivity is similar to that of H_2SO_4 [e.g., Lide, 2008]. Following Mulvaney *et al.* [1988], we now assume that the grains are spherical and that the triple junctions are cylindrical. The measured mean cross-sectional area of the grains

(1.8 mm²) implies that their diameter is 1.8 mm and that the triple-junction diameter is 0.8 μm. Together, these data and empirical models lead to $\sigma_{DC} = \sim 6 \times 10^{-11} \text{ S m}^{-1}$ at -20°C (Figure 2). This calculation also assumes that there is 7 μM of H₂SO₄ in the bulk sample but that it is concentrated at the triple junctions, which form a continuous yet tortuous path similar to that of laboratory-frozen ices [Grimm *et al.*, 2008] or consolidated geologic materials [Keller, 1982]. It should thus be considered an upper bound for σ_{DC} for meteoric ice. The modeled σ_{DC} fits neither the temperature dependence nor the magnitude of our observed values of σ_{DC} (Figure 2).

5.2. Migration of Protonic Point Defects Through Polycrystalline Ice

[36] Having shown above that electrolytic grain-boundary conduction does not describe our data adequately, we now reconsider intracrystalline conduction following Jaccard theory. ECM data suggest that the low-frequency conductivity of polar ice ($\sim\sigma_{DC}$) at $\sim-15^\circ\text{C}$ depends on [H⁺] only [Wolff *et al.*, 1997], which implies that σ_{\pm} dominates σ_{DC} , i.e., σ_{\pm} is consistently less than σ_{DL} . However, Jaccard theory does not account for the grain boundaries in polar ice, which interrupt the ordered ice lattice through which protonic point defects must migrate to conduct charge at DC. If polycrystalline ice is equivalent to a series circuit comprised of both static crystal and grain-boundary “resistors” (σ_s and σ_{gb} , respectively), then σ_{DC} will be dominated by the least conductive element. As shown in the previous section, even if the triple junctions are always acid-filled and liquid, their contribution to bulk DC conductivity is too small to explain observed σ_{DC} values, so σ_{gb} likely dominates σ_{DC} . This result also implies that $\sigma_s > \sigma_{gb}$.

[37] The temperature dependence of σ_{DC} offers an additional clue as to the nature of the DC conduction mechanism. Our laboratory measurements yielded $E_{DC} = 0.98 \pm 0.25 \text{ eV}$ (Figure 2). This range is consistent with previous measurements of laboratory-frozen, doped polycrystalline ice (0.7–1 eV) [Grimm *et al.*, 2008]. From “DC” georesistivity surveys, Reynolds and Paren [1984] and Shabtaie and Bentley [1995] inferred $E_{DC} = 0.15\text{--}0.25 \text{ eV}$, while Hammer [1980] and Taylor *et al.* [1992] inferred that $E_{DC} = 0.18\text{--}0.45 \text{ eV}$ from ECM. Wolff *et al.* [1997] observed that this range for E_{DC} was inconsistent with the apparent activation energy of the conductivity of ionic defects ($E_{\pm} = 0 \text{ eV}$) in doped, single crystals of ice at high temperatures, implying that intracrystalline conduction is insignificant. However, the two key studies that investigated the behavior of ionic defects reported conflicting values for this activation energy (up to 0.36 eV, depending on ionic defect concentration) [Camplin *et al.*, 1978; Takei and Maeno, 1987]. As discussed earlier, the conductivity values reported from georesistivity surveys are not representative of σ_{DC} (Figure 2), so we discard any inference of the value of E_{DC} from them. The E_{DC} range we observed is much greater than the activation energies of either ionic or Bjerrum defects [e.g., Petrenko and Whitworth, 1999; Grimm *et al.*, 2008], which suggests that an additional process impedes DC conduction in meteoric ice, of which the most plausible possibility is the grain boundaries.

[38] Grimm *et al.* [2008] found that σ_{DC} increased and E_{DC} decreased significantly above the eutectic temperature for ice samples frozen from salt solutions greater than 3 mM, which implies that the dominant conduction mechanism switched

to electrolytic grain-boundary conduction. Only one of our ice core samples showed similar evidence of a eutectic-related change in complex permittivity (Figure 4). This result suggests that, for the majority of our samples, σ_{DC} is limited by the low conductivity of the acid and/or salt hydrates at grain boundaries. In other words, the electrical behavior of the ice-core sample shown in Figure 4 is the exception to the rule. We are aware of only one other study that found evidence of a eutectic-related change in conductivity for acidic polar ice, specifically in σ_{∞} [Fujita *et al.*, 2002], which was much smaller than what we observed. This change also occurred at a lower temperature (-81°C , which does not correspond to any individual acid or salt eutectic temperature), where electrolytic grain-boundary conduction might dominate (Figure 2), but which is well below the range of terrestrial ice-sheet temperatures.

[39] Given the above evidence, we conclude that DC conduction in polar ice occurs by migration of protonic point defects through the ice lattice and grain-boundary hydrates, but that it is impeded by the significant resistance associated with grain boundaries. The activation energy of this sequence is equal to the largest of the activation energies of its component mechanisms. For the ice lattice, it is $\sim 0\text{--}0.36 \text{ eV}$, but it is much higher when entering and exiting the hydrate ($\sim 0.7\text{--}1 \text{ eV}$) [Grimm *et al.*, 2008]. If grain-boundary hydrates were sufficiently conductive and well connected, then the series-circuit sequence described above would break down and such grain boundaries would short out intracrystalline conduction in the ice lattice. This alternative scenario is analogous to that of liquid acid-filled grain boundaries, which we modeled above (equation (12)). Hence, we consider it unlikely.

[40] The validity of our suggested DC conduction mechanism (migration of protonic point defects impeded by grain boundaries) increases with evidence of protonic point defects in the lattice of polar ice. There is substantial indirect evidence that Cl⁻ and NH₄⁺ regularly form Bjerrum defects [e.g., Moore *et al.*, 1992b, 1994a, 1994b; Barnes and Wolff, 2004], but no equivalent evidence of ionic defects in polar ice exists. By examining the temperature dependence of the dielectric susceptibility $\Delta\epsilon'$, our data provide an additional test for both types of defects. Assuming that the temperature dependencies of the defect mobilities are not equal, then following equation (7), any significant reduction in $\Delta\epsilon'$ (relative to that of ice containing only one defect type) or change in temperature dependence implies that both defect types are present.

[41] Figure 6 shows an example of the determination of $\Delta\epsilon'$ from complex permittivity data and summarizes the temperature dependence of all observed dielectric relaxations in our ice core samples. We typically observed two near-Debye dielectric relaxations and sometimes three. We hypothesize that the multiple relaxations are caused by multiple populations of crystals with differing concentrations of protonic point defects, and consider the implications of this hypothesis later (section 7.2). Regardless of the nature of the multiple relaxations, the reduced $\Delta\epsilon'$ values we observed imply that both ionic and Bjerrum defects are typically present in polar ice [Takei and Maeno, 1987; Petrenko and Whitworth, 1999]. The decrease in $\Delta\epsilon'$ with decreasing temperature also implies that both defect types are present, because the only plausible explanation for this behavior is that σ_{\pm} and σ_{DL}

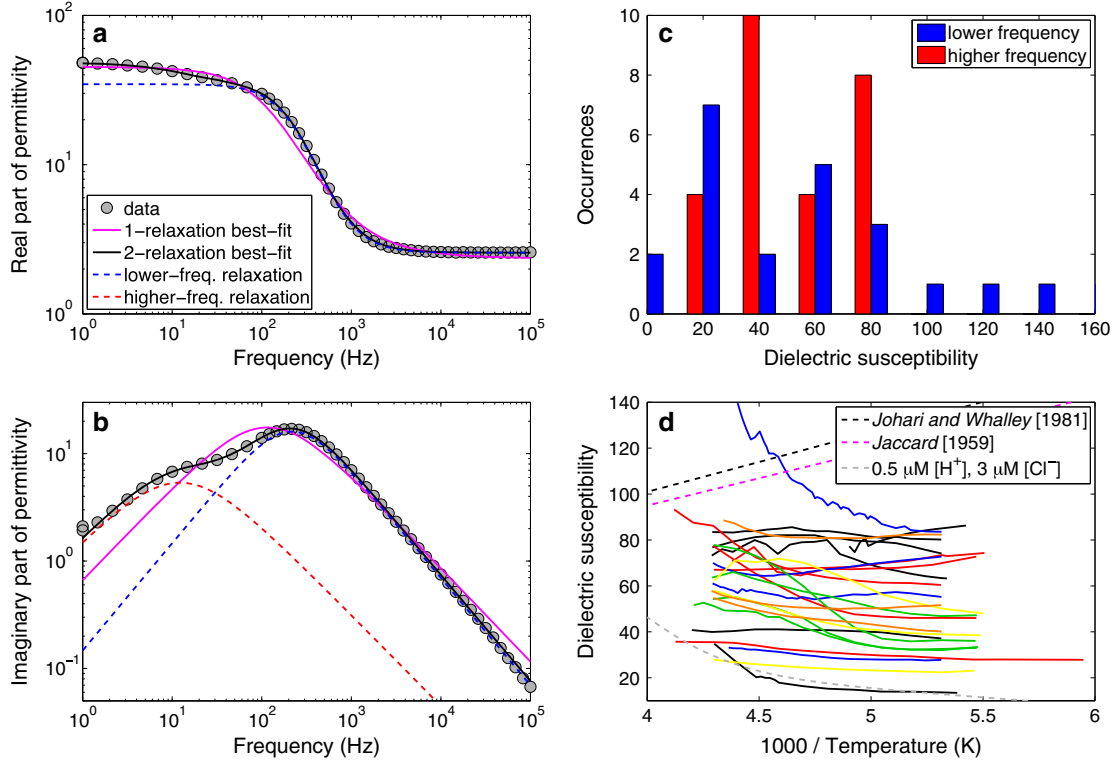


Figure 6. (a, b) Example Cole—Cole modeling of the complex permittivity 89.01-m South Pole sample. These data are best fit by two near-Debye relaxations, rather than a single Debye relaxation. (c) Histogram of observed lower- and higher-frequency relaxation values of $\Delta\epsilon'$ at -85°C . (d) The temperature dependence of $\Delta\epsilon'$ for the higher-frequency relaxation of all ice core samples. Colors follow those for Figure 1a–c. Predictions of the temperature-dependent behavior of $\Delta\epsilon'$ from Jaccard [1959] and Johari and Whalley [1981] for ice containing only L-defects do not match the observed temperature dependence. An example prediction using equation (7) (gray line) assumes non-zero concentrations of both defect types and matches the data better.

converge at lower temperatures (equation (7)). This behavior diverges from that of ice doped with L-defects only [Jaccard, 1959; Johari and Whalley, 1981], but is similar to that predicted for ice containing both defect types (Figure 6d).

6. Interpretation of Ice Core Electrical Logs

[42] Having shown above that DC conduction in polar ice is best explained by the behavior of protonic point defects, rather than electrolytic conduction, we next consider the implications of these results for electrical logs of ice cores. We first revisit interpretations of DEP logs in terms of Jaccard theory, and then use that analysis to better interpret ECM signals. We focus here on ECM and DEP, as these are the two primary electrical logging methods.

6.1. Relationship Between Jaccard Theory and DEP

[43] The DC conductivity of polar ice is too small to explain any significant portion of the HF conductivity of ice (Figure 2), contrary to the suggestion made by Wolff *et al.* [1997]. This suggestion was predicated on the validity of the georesistivity surveys as a DC conductivity measurement and the interpretation of those surveys in terms of the parallel-circuit electrolytic conduction model (equation (11)).

[44] At frequencies well above the Debye relaxation, i.e., HF, grain boundaries should not impede conduction because at these frequencies protonic point defects cannot reorient quickly enough to remain in-phase with the alternating electric field. The frequency above which conduction is no longer affected by grain boundaries is the minimum Debye frequency at which the integrated effect of the multiple Debye relaxations can be discerned from the imaginary part of the permittivity. From Figure 1, a typical value for this “transition” frequency at -40°C is between 10 and 100 Hz, although it can exceed 10^3 Hz at -10°C . We thus hypothesize that equation (10), an empirical relationship between bulk impurity concentrations and DEP-measured σ_∞ for polar ice at -15°C , can be fully expressed in terms of Jaccard theory. This analysis has already been partially done for Cl^- and NH_4^+ [Moore *et al.*, 1994a], but not for H^+ .

[45] We first correct each defect’s mobility to $T_0 = -15^\circ\text{C}$ using the appropriate defect activation energy (Table 1) as

$$\mu_i = \mu_0 \frac{T_0}{T} \exp \left[\frac{E_i}{k} \left(\frac{1}{T_0} - \frac{1}{T} \right) \right], \quad (13)$$

where μ_0 is the mobility at T_0 . The mobility and activation energy of L- and D-defects are better constrained than for extrinsic ionic H_3O^+ defects. We chose an intermediate value for E_\pm (0.21 eV; Table 1) that is within the reported

range at these temperatures (0–0.36 eV [Camplin *et al.*, 1978; Takei and Maeno, 1987]). To relate Jaccard theory to equation (10), we consider several cases, depending on the impurities present. Below we describe the pure ice and H^+ -only cases, and we summarize all scenarios in Table 3.

[46] The response of HF conductivity at -15°C to H^+ is much larger than that of Cl^- per unit concentration. From the empirical equation (10), this ratio is ~ 7 ; a synthesis of reported data by MacGregor *et al.* [2007] gives a ratio of ~ 6 – 9 . Interestingly, this ratio is consistent with that predicted by Jaccard theory in terms of the products of the defect charges and mobilities:

$$\frac{\mu_{H_3O^+} e_{\pm}}{\mu_{exL} e_{DL}} \approx 8. \quad (14)$$

[47] Given earlier work that explained the DEP response to Cl^- in terms of Jaccard theory [e.g., Moore *et al.*, 1992a], this coincidence implies that Jaccard theory also explains the role of acids in HF conduction adequately.

[48] Equation (10) implies that the conductivity of pure ice at -15°C is $9 \mu\text{S m}^{-1}$. Following equation (1),

$$n_{inL} = \frac{9}{\mu_{inL} e_{DL}}, \quad (15)$$

which yields an intrinsic L-defect concentration (n_{inL}) of $\sim 4 \times 10^{21} \text{ m}^{-3}$. This value is close to that derived from other experimental data ($\sim 3 \times 10^{21} \text{ m}^{-3}$) [Petrenko and Whitworth, 1999].

[49] If H^+ is the only lattice-soluble impurity present, then equation (10) reduces to $\sigma_{\infty} = 9 + 4 [H^+]$. This relationship assumes that H^+ enters the ice lattice without a lattice-soluble anion. An insoluble anion must therefore be enclathrated, and the H^+ ion creates one ionic defect (H_3O^+) and one D-defect. However, $\mu_{H_3O^+} \gg \mu_D$, so we ignore the conductivity contribution from D-defects. In terms of Jaccard theory, this relationship can be expressed as

$$\sigma_{\infty} = 9 + 4 [H^+] = n_{inL} \mu_{inL} e_{DL} + n_{\pm} \mu_{H_3O^+} e_{\pm}. \quad (16)$$

Table 3. Modeled Partitioning of Impurities into the Lattice of Polar Ice Based on the GRIP Chemistry—DEP Relationship

Ions Present	Extrinsic Defects Created (per ion set) ^a	Partition Coefficient (%)
NH_4^+, Cl^-	2 D, 2 L	80
H^+, Cl^-	1 H_3O^+ , 1 L	55
Cl^-	2 L	30
NH_4^+	2 D	$\leq 80^b$
H^+	1 H_3O^+ , 1 D	55

^aIntrinsic Bjerrum L-defects are present in all scenarios. For a given impurity scenario, we assume that all possible cosubstitutions occur first, that like defects (i.e., NH_4^+ and Cl^-) cosubstitute together first, and that any remaining impurities substitute into the lattice at their lower individual partition coefficients. The order of preference for cosubstitution is from the top of the table to the bottom. For example, if all three lattice-soluble impurities are present, then $\sim 80\%$ of available NH_4^+ and Cl^- , $\sim 55\%$ of the H^+ and the remaining Cl^- enter the lattice, and so forth.

^bCalculated value is 680%, which is nonphysical. Its true value must be less than or equal to 80%, i.e., the calculated value when both NH_4^+ and Cl^- cosubstitute into the lattice.

[50] We ignore the pure ice component of the DEP relationship, as it appears well explained by intrinsic L-defects (equation (15)). Equation (16) thus reduces to

$$n_{\pm} = 4 \frac{[H^+]_{bulk}}{\mu_{H_3O^+} e_{\pm}}. \quad (17)$$

[51] We add the subscript “bulk” to $[H^+]$ to emphasize that the concentration originally referred to in equation (10) is that of the bulk ice sample, not just the ice lattice. Dimensional analysis shows that

$$\begin{aligned} n_{\pm} &= 1 \frac{\text{defect}}{\text{molecule}} \times [H^+]_{lattice} \frac{\text{mol}}{\text{L}} \times N_A \frac{\text{molecule}}{\text{mol}} \times 1000 \frac{\text{L}}{\text{m}^3} \\ &= 1000 N_A [H^+]_{lattice} \frac{\text{defect}}{\text{m}^{-3}}, \end{aligned} \quad (18)$$

where N_A is the Avogadro constant ($6.02214 \times 10^{23} \text{ mol}^{-1}$) and $[H^+]_{lattice}$ is the concentration of H^+ in the ice lattice. We can then determine the partition coefficient γ between the lattice and bulk concentrations of H^+ as

$$\gamma_{H^+} = \frac{[H^+]_{lattice}}{[H^+]_{bulk}} = \frac{4}{1000 N_A \mu_{H_3O^+} e_{\pm}}. \quad (19)$$

[52] For H^+ only, this analysis suggests that, on average, $\sim 55\%$ of $[H^+]_{bulk}$ is in the lattice in the GRIP ice core, with the remainder presumably at the grain boundaries and/or localized inclusions. Furthermore, we predict that enhanced impurity partitioning should occur when lattice-soluble counterions are present, i.e., it is more energetically favorable to introduce a lattice-soluble counterion into the ice lattice than to enclathrate an insoluble counterion (Table 3). This prediction is supported by observations of the enhanced lattice solubility of Cl^- and NH_4^+ when both are present in frozen solutions [Gross *et al.*, 1977; Stillman *et al.*, 2013]. In the case of NH_4^+ , this approach yielded an unrealistic partition coefficient ($>100\%$). The coefficient for $[NH_4^+]$ in equation (10) is likely affected by the cosubstitution of NH_4^+ and Cl^- , i.e., the presence of available Cl^- increases the partitioning of NH_4^+ into the ice lattice [Stillman *et al.*, 2013]. Our estimates of soluble ion partitioning in meteoric ice are consistent with previous estimates, e.g., 30–70% for Cl^- for the Dolleman Island ice core [Moore *et al.*, 1992b] (which has low $[NH_4^+]$) and more than 75% for NH_4^+ for the GRIP ice core [Moore *et al.*, 1994a].

6.2. Relationship Between Jaccard Theory and ECM

[53] Having “calibrated” the partitioning of each lattice-soluble impurity using the GRIP chemistry—DEP relationship (equation (10)), we can now calculate the static conductivity of a single grain, σ_s (equation (4)), and explore its possible relationship with ECM signals. We hypothesize that ECM responds to the static conductivity of the ice crystals (σ_s) instead of the bulk σ_{DC} value, which is lower due to grain boundaries. The electric fields imposed by ECM are so large ($\sim 10^5 \text{ V m}^{-1}$) that dielectric breakdown is likely across grain boundaries, shorting out their resistance. This hypothesis is supported qualitatively by the smell of ozone that is sometimes reported during ECM logging [Hammer, 1983],

caused presumably by arcing of free charges along grain boundaries.

[54] Jaccard theory predicts that the static conductivity of ice is nonlinearly related to the concentrations of both ionic and Bjerrum defects. However, this static conductivity depends only weakly on the presence of extrinsic Bjerrum defects, because their concentrations in polar ice are low compared to those that are intrinsic to pure ice (Figure 7). The key to understanding the behavior of σ_s is to recognize that σ_{DL} depends on the concentrations of all Bjerrum defects, including intrinsic L-defects. Equation (4) is thus expressed more clearly as

$$\frac{e^2}{\sigma_s} = \frac{e_{\pm}^2}{\sigma_{\pm}} + \frac{e_{DL}^2}{\sigma_{exD} + \sigma_{inL} + \sigma_{exL}}. \quad (20)$$

[55] At -15°C , σ_s depends on σ_{exL} when $\sigma_{exL} > \sigma_{inL}$, which occurs only when $[\text{Cl}^-]_{bulk} > \sim 18 \mu\text{M}$ (Figure 7). Because such concentrations are rare in meteoric polar ice, σ_s is virtually independent of $[\text{Cl}^-]_{bulk}$ (Figure 8). Such concentrations can occur in marine ice, but no ECM- $[\text{H}^+]$ data for marine ice are available to test this prediction, and electrolytic conduction due to interconnected brine channels occurs at very high values of $[\text{Cl}^-]_{bulk}$ ($> \sim 300 \mu\text{M}$) [Moore *et al.*, 1994b].

[56] Jaccard theory also predicts that σ_s is nonlinearly related to n_{\pm} and thus $[\text{H}^+]_{lattice}$ (Figure 9). This relationship thus offers a simple explanation for the nonlinearity of the relationship between ECM current and $[\text{H}^+]_{bulk}$. Current density \vec{J} is related to σ_s and the applied electrical field \vec{E}

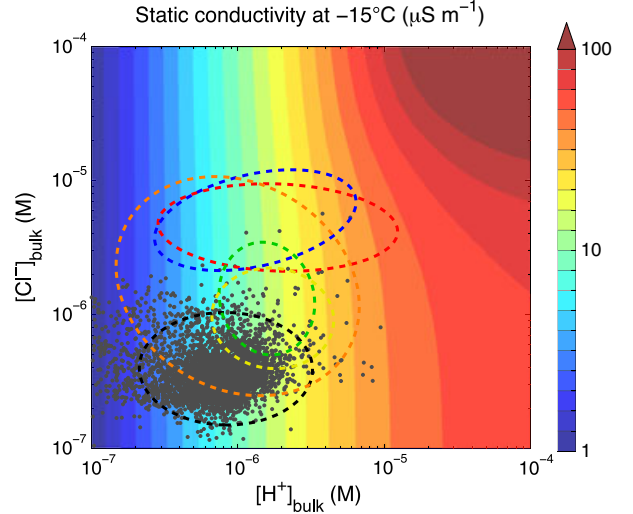


Figure 8. Modeled response of the static conductivity of polar ice (σ_s) to bulk impurity concentrations. The partitioning of H^+ and Cl^- into the ice lattice is inferred from the chemistry—DEP relationship for the GRIP ice core (equation (10); Table 3). Points are bulk impurity concentration data from the nearby GISP2 ice core [Yang *et al.*, 1997]. Dashed ellipses are the 95% confidence regions for non-zero impurity concentrations for the ice cores we studied; color key again follows Figures 1a–c. Impurity concentrations in polar ice are rarely high enough for the static conductivity to depend clearly on the concentration of Cl^- .

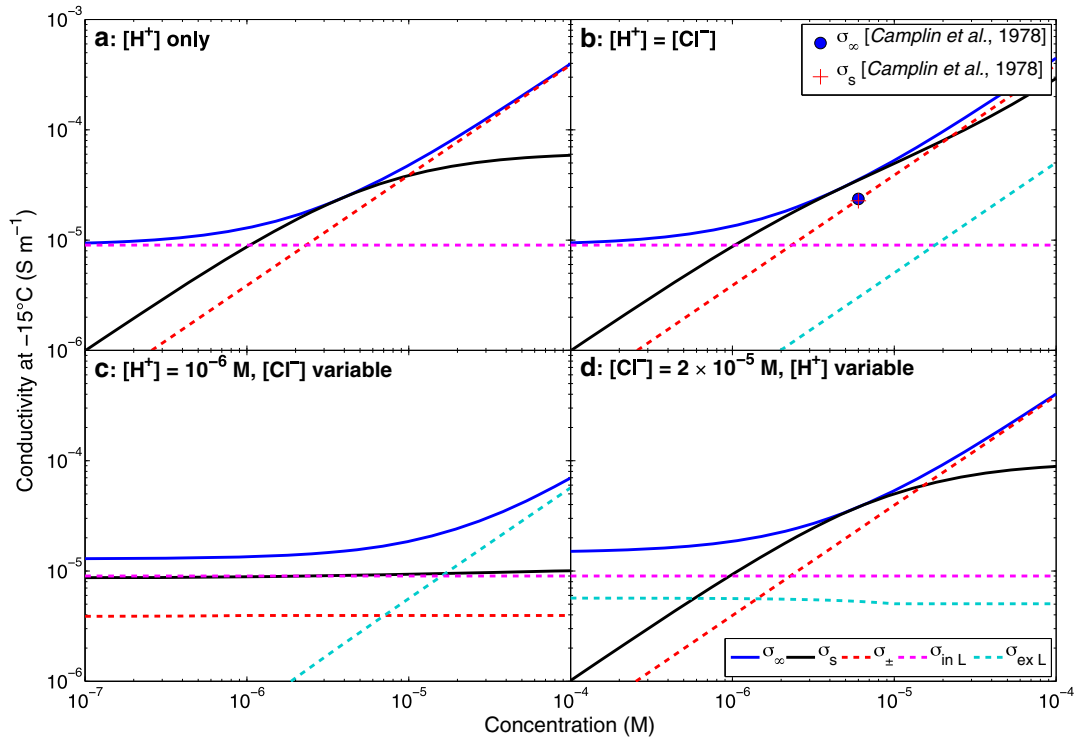


Figure 7. (a–d) Jaccard conductivities as a function of $[\text{H}^+]_{bulk}$ and $[\text{Cl}^-]_{bulk}$. Four different bulk impurity concentration scenarios are considered at -15°C . In all cases, σ_s depends only weakly on σ_{exL} , which is related directly to $[\text{Cl}^-]_{bulk}$. Data from Camplin *et al.* [1978] are shown in Figure 7b; they froze a 6- μM hydrofluoric acid solution (F^- behaves similarly to Cl^- in the lattice).

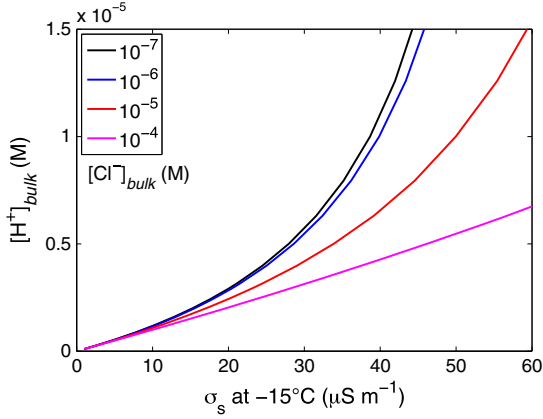


Figure 9. Relationship among static conductivity (σ_s), $[\text{H}^+]_{\text{bulk}}$, and $[\text{Cl}^-]_{\text{bulk}}$, again assuming the impurity partitioning inferred from equation (10) (Table 3). As $[\text{Cl}^-]_{\text{bulk}}$ increases, the nonlinearity between σ_s and $[\text{H}^+]_{\text{bulk}}$ decreases, which is consistent with the relationship between two single-core ECM- $[\text{H}^+]_{\text{bulk}}$ calibrations.

as $\vec{J} = \sigma_s \vec{E}$. Thus, the nonlinear relationship between σ_s and $[\text{H}^+]_{\text{lattice}}$ should also be expressed by the current recorded by ECM. Assuming constant partitioning of H^+ into the lattice, ECM conductance is also nonlinearly related to $[\text{H}^+]_{\text{bulk}}$.

[57] Finally, Jaccard theory can also explain the variability of ECM- $[\text{H}^+]_{\text{bulk}}$ calibrations for polar ice cores [Moore et al., 1992a, 1994a]. As n_{exL} increases (i.e., increasing $[\text{Cl}^-]_{\text{lattice}}$), the relationship between σ_s and n_{\pm} becomes more linear (Figure 9). Again assuming constant partitioning, ice cores with larger mean values of $[\text{Cl}^-]_{\text{bulk}}$ should have ECM- $[\text{H}^+]_{\text{bulk}}$ calibrations that are more linear. For the GRIP ice core from central Greenland, the power law exponent for the ECM- $[\text{H}^+]_{\text{bulk}}$ calibration is ~ 2 [Moore et al., 1994a], and the mean value of $[\text{Cl}^-]_{\text{bulk}}$ in the nearby GISP2 ice core is $1.2 \mu\text{M}$ [Yang et al., 1997]. At Dolleman Island in the Antarctic Peninsula, the power-law exponent is $0.62\text{--}1.48$, depending on the assumptions used, and the mean value of $[\text{Cl}^-]_{\text{bulk}}$ is greater than $10 \mu\text{M}$ [Moore et al., 1992b]. Although this analysis cannot be considered a rigorous test of our ECM- σ_s hypothesis, because both the sampling and calibration methods differed at both sites, the data are consistent with our prediction based on Jaccard theory. For low values of $[\text{H}^+]_{\text{bulk}}$, the relationship is mostly linear and unaffected by $[\text{Cl}^-]_{\text{bulk}}$. However, unless a robust regression is used, a nonlinear regression will be sensitive to high acidity values ($>10 \mu\text{M}$) where the value of σ_s is affected more strongly by $[\text{Cl}^-]_{\text{bulk}}$ (Figure 9).

[58] From this analysis, we conclude that ECM remains an invaluable tool for high-resolution electrical characterization of ice cores [e.g., Taylor et al., 1993]. However, its response is not representative of bulk DC conduction, and it is sensitive primarily to a single type of protonic point defect, whereas DEP responds clearly to all defect types.

7. Discussion

7.1. “DC” Georesistivity Surveys

[59] The similarity between the georesistivity data and our σ_{∞} data in terms of both magnitude and temperature

dependence suggests that those surveys actually measured σ_{∞} . These discrepancies could be due to the difference in measurement scale. Georesistivity surveys on ice sheets typically measured σ_{DC} across scales of several hundreds of meters, whereas laboratory measurements are made across scales of several centimeters. However, radar sounding probes ice at comparable spatial scales to georesistivity surveys. Depth-averaged attenuation rates (related to σ_{∞}), inferred from radar sounding are generally consistent with the empirical σ_{∞} models used in Figure 5 [e.g., MacGregor et al., 2007, 2011; Jacobel et al., 2009, 2010; Matsuoka et al., 2012]. The success of these models suggests that σ_{∞} is scale-independent and, by inference, that σ_{DC} is also scale-independent. Because of the challenge of measuring σ_{DC} in polar ice sheets, there is no clear evidence of its scale independence beyond the data synthesis described in section 4.1. However, no DC conduction mechanism has been proposed that would clearly be scale-dependent between 10^{-2} and 10^2 m.

[60] We hypothesize that past georesistivity surveys of polar ice sheets did not measure the DC conductivity accurately because of the high contact impedance of the near-surface firn where electrodes were situated. This impedance makes injecting sufficient current challenging and necessitated experimental compromises [Reynolds and Paren, 1984; Shabtaie and Bentley, 1995], such as measuring the response of a discharging resistor-capacitor system and not that of a resistor only, which introduced a near-HF response. As evidenced by our broadband data (e.g., Figure 1e), any measurement of conductivity at a frequency higher than ~ 50 Hz is also influenced by the primary Debye relaxation and should not be considered a DC measurement.

[61] Georesistivity surveys of temperate glaciers are typically undertaken in the ablation zone, where more manageable contact resistances are possible when electrodes are situated in melt ponds [e.g., Keller and Frischknecht, 1960] as compared to surveys over polar firn. The relatively lower contact impedance allows the georesistivity measurements to be made normally, i.e., a constant current is injected into the current electrodes, while a steady voltage is measured at the potential electrodes. Such surveys have found that the upper 20 m of temperate glaciers is more conductive ($\sigma_{\text{DC}} \sim 0.6\text{--}18 \mu\text{S m}^{-1}$) than a deeper, more resistive zone ($\sigma_{\text{DC}} \sim 0.006\text{--}0.3 \mu\text{S m}^{-1}$), due to liquid water in the shallow zone [Kulesa, 2007]. The upper range of those measurements is comparable to the range we predict ($\sim 0.5\text{--}5 \mu\text{S m}^{-1}$) for meteoric polar ice at 0°C from our data (Figure 2). We suggest that deeper temperate ice is less conductive than either polar or shallow temperate ice due to reorganization of impurity-laden ice lattices during recrystallization [Kulesa, 2007], annealing, or perhaps flushing of impurities [Glenn et al., 1977]. Fitzgerald and Paren [1975] showed that melting and then refreezing polar ice causes a significant drop in σ_{∞} . This behavior occurs presumably because partitioning of soluble impurities into the ice lattice is dramatically lower (3 orders of magnitude) after refreezing [Gross et al., 1977]. This partitioning difference is probably due to the quenching or rapid freezing that occurs in the polar atmosphere. With fewer soluble impurities forming defects in temperate ice, both σ_s and σ_{DC} will decrease. Defects are more likely to anneal out at the near-melting temperatures

of temperate ice and over the multidecadal residence time of ice in non-polar glaciers.

7.2. Impurity Partitioning in Polar Ice

[62] Jaccard theory is the only viable explanation for the role of acids as the dominant impurity in conduction through polar ice. This conclusion has important implications for investigations of impurity partitioning in polar ice, because all impurities that increase ice conductivity can now be understood in terms of this theory. For example, our analysis of the GRIP ice core’s relationship between chemistry and DEP logs (equation (10)) suggests that, on average, more than half of these impurities remain at grain boundaries in the GRIP ice core (Table 3). A combination of chemistry, ECM, and DEP logs can now be interpreted explicitly in terms of the partitioning of H^+ , Cl^- , and NH_4^+ between the ice lattice and grain boundaries and/or inclusions. Because ECM responds to acids only, it can help distinguish the DEP response of ionic defects from that of Bjerrum defects. Reduction of DEP-measured HF conductivity to defect concentrations using Jaccard theory could be used to produce “partitioning logs” for H^+ , Cl^- , and NH_4^+ .

[63] The partition coefficient of meteoric polar ice is far greater than the equilibrium partition coefficient (2.7×10^{-3}) measured for slowly frozen laboratory-grown ice [Gross *et al.*, 1977; Grimm *et al.*, 2008]. We speculate that the degree of partitioning of these impurities in polar ice varies with depositional environment and postdepositional processes. The GRIP chemistry—DEP relationship (equation (10)) is thus unlikely to apply universally to polar ice, because the nature of impurity deposition in polar regions varies widely [Wolff *et al.*, 1998]. For example, one possibility is that the degree of partitioning is related to each impurity’s primary deposition mechanism, i.e., dry (aerosol) or wet (snowfall). Further investigation into the spatiotemporal variability of impurity partitioning in ice is now both feasible with available tools (electrical and chemical logs and microstructural analysis) and warranted, because it has the potential to provide additional insight into the nature of past changes in polar atmospheric chemistry.

[64] A final aspect of our data that warrants further investigation is the observation that meteoric polar ice often possesses more than one dielectric relaxation between DC and HF (Figure 6). Fitting our complex permittivity spectra with a single relaxation (equation (8)) results in a poorer fit for 24 of our 26 samples. In the case of at least one sample from GISP2, three distinct dielectric relaxations are observed (Figure 10). A comparison of our inferred relaxation frequencies with those of laboratory-frozen ice suggests a relationship between these multiple relaxations and impurity partitioning. The lower-frequency relaxation of meteoric polar ice often matches that of ice frozen from ultrapure water, while its higher-frequency relaxation often approaches that of ice saturated with L-defects formed by Cl^- (Figure 10). The frequency of both relaxations nearly always falls within the established range between pure ice and Cl^- -saturated ice, except where Cl^- co-substitutes into the lattice with NH_4^+ , as appears to be the case for the GISP2 sample shown in Figure 10.

[65] These relationships imply that there are typically two populations of crystals in meteoric polar ice: one that contains very few extrinsic defects (ionic or Bjerrum), and another that contains a larger concentration thereof. The

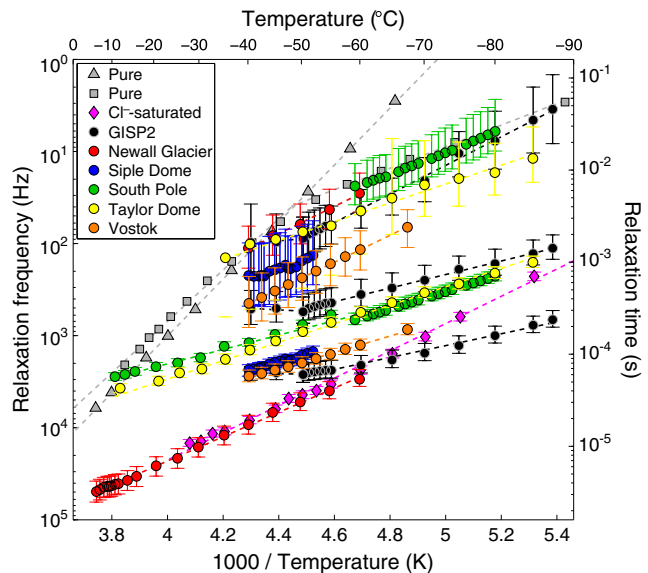


Figure 10. Temperature dependence of the multiple dielectric relaxations of six of our ice core samples (the same samples shown in Figure 1a–c). Also shown are classic measurements of laboratory-frozen pure ice (triangles: [Auty and Cole, 1952]; squares: [Kawada, 1978]) and Cl^- -saturated ice frozen from a 850-mM NaCl solution [Grimm *et al.*, 2008]. Error bars represent the 95% confidence intervals for each value where available.

combination of the electrical properties of these two crystal populations produces the bulk electrical behavior observed. A suitable mixing model is thus required to predict bulk electrical properties from multiple crystal populations, and its form for polar ice is not yet clear. Regardless, this observation appears to be fundamental to the microstructure of polar ice. We speculate that the observed variability in the magnitude of these multiple relaxations is also related to each sample’s formation and postdepositional history, and thus may also inform future investigations of impurity partitioning.

7.3. Implications for Radar Sounding

[66] Improving englacial radar attenuation models is of increasing importance, as glaciologists seek to better understand the nature of ice sheet beds from radar sounding and ultimately improve predictions of the contribution of ice sheets to sea-level rise. Our discovery of the broad applicability of Jaccard theory to the interpretation of HF conduction in polar ice thus also affects analysis of radar soundings of ice masses. Attenuation of radio waves in ice is related directly to σ_∞ [e.g., MacGregor *et al.*, 2007; Figure 1f]. Experiments aimed at further constraining the charge, mobility and partitioning of protonic point defects (i.e., the key parameters in Jaccard theory; Table 1) will therefore lead directly to improvements in radar-attenuation models. The empirical relationships between chemistry and σ_∞ described by Wolff *et al.* [1997] and MacGregor *et al.* [2007] are essentially simplified expressions of Jaccard theory for HF only, implicitly corrected for impurity partitioning in polar ice.

[67] We speculated above that variable impurity partitioning in ice is related to the nature of impurity deposition. The mode

of impurity deposition (dry or wet) has recently been shown to have a non-negligible effect upon englacial radar-attenuation predictions [MacGregor *et al.*, 2012]. Hence, improving understanding of the nature of impurity deposition onto polar ice sheets may also have direct value to radar sounding of ice sheets.

8. Conclusions

[68] We comprehensively investigated the two existing hypotheses regarding the role of acids in DC and HF conduction in polar ice and found that both our observations and the behavior of electrical logs of ice cores are well explained by the migration of charged protonic point defects, with an additional DC impedance associated with grain boundaries. “DC” georesistivity surveys are inconsistent with both our data and those of others regarding the electrical properties of polar ice. The hypothesis that acids conduct electrolytically along grain boundaries was based on a subset of those georesistivity surveys. While this hypothesis is consistent with some microstructural observations of meteoric ice, it is inconsistent with both our observations and the electrical behavior of similar geologic materials.

[69] At typical bulk impurity concentrations in meteoric polar ice, its HF conductivity is the sum of contributions from ionic defects due to acids, extrinsic Bjerrum defects due to Cl^- and NH_4^+ , and Bjerrum defects intrinsic to pure ice. This behavior is consistent with existing empirical HF conductivity models and the DEP response to impurities. ECM measurements respond to bulk acidity only because, at typical meteoric polar ice concentrations and logging temperatures, the conductivity contribution from intrinsic Bjerrum defects is much higher than that of extrinsic Bjerrum defects. Thus, only variability in the concentration of ionic defects clearly affects the static conductivity to which ECM responds. ECM conductance should not be considered a measure of bulk DC conductivity.

[70] These observations and analysis directly affect studies of paleoclimate from ice cores and radar sounding of ice sheets. By reconciling Jaccard theory with the behavior of electrical logs of ice cores and empirical relationships for HF conductivity, we now recognize that the primary unknown in parameterization of conduction mechanisms in polar ice is impurity partitioning. Future investigation of the spatiotemporal variability of this partitioning using electrical measurements will clarify its possible relationship to paleoclimate beyond what has been possible with direct microstructural investigations alone.

Notation

[71] $\sigma_{\pm}, \sigma_{\text{DL}}$	conductivities due to ionic and Bjerrum defects, respectively
$\sigma_{\text{H}_3\text{O}^+}, \sigma_{\text{OH}^-}$,	conductivities of the mobilities of extrinsic H_3O^+ , extrinsic OH^- ,
$\sigma_{\text{inL}}, \sigma_{\text{inD}}, \sigma_{\text{exL}}, \sigma_{\text{exD}}$	intrinsic Bjerrum L-defects, intrinsic Bjerrum D-defects, extrinsic Bjerrum L-defects, and Bjerrum D-defects, respectively

n	defect concentration
μ	defect mobility
e	elementary charge ($1.602 \times 10^{-19} \text{ C}$)
e_{\pm}, e_{DL}	charges of ionic ($\pm 0.62e$) and Bjerrum (DL $0.38e$) defects, respectively
σ_s	static conductivity of a single ice crystal
τ	relaxation time
T	temperature
f_r	relaxation frequency
$\Delta\epsilon'$	dielectric susceptibility
ϵ_0	permittivity of the vacuum ($8.854 \times 10^{-12} \text{ F m}^{-1}$)
σ_{∞}	HF-limit conductivity
ϵ^*	complex relative permittivity
ϵ', ϵ''	real and imaginary parts of ϵ^*
i	$\sqrt{-1}$
ϵ_{∞}	HF-limit permittivity
ω	angular frequency
α	Cole—Cole distribution parameter
σ_{DC}	DC conductivity
k	Boltzmann constant ($8.617 \times 10^{-5} \text{ eV K}^{-1}$)
σ_{DC}^0	DC conductivity at a reference temperature
T_0	reference temperature
S	relative saturation
β	saturation exponent
σ_{liq}	DC conductivity of the liquid matrix
ϕ	bulk porosity
m	cementation exponent
w	Triple-junction radius
D	grain diameter
E_{DC}	activation energy of DC conductivity
$E_{\text{inL}}, E_{\pm}, E_{\text{exL}}, E_{\text{exD}}$	activation energies of the mobilities of intrinsic Bjerrum L-defects and extrinsic ionic, Bjerrum L-, and Bjerrum-D defects, respectively
σ_{gb}	grain-boundary conductivity
μ_0	defect mobility at T_0
γ	partition coefficient, i.e., ratio between impurity concentration in the lattice and the bulk impurity concentration
\vec{J}	current density
\vec{E}	applied electric field

[72] **Acknowledgments.** This work was supported by the Planetary Geology and Geophysics Program, National Aeronautics and Space Administration (grants NNX10AJ65G and NNX08AM92G). We thank the innumerable individuals who collected and first studied these ice cores, the U.S. National Ice Core Laboratory for providing the ice core samples, and D. D. Blankenship, K. L. Neal, and D. P. Winebrenner for valuable

discussions. We also thank Associate Editor J. N. Bassis, S. A. Arcone, and two anonymous reviewers for constructive comments that improved the manuscript.

References

- Archie, G. E. (1942), The electrical resistivity log as an aid in determining some reservoir characteristics, *Petrol. Trans. AIME*, *146*, 54–62.
- Auty, R. P., and R. H. Cole (1952), Dielectric properties of ice and solid D₂O, *J. Chem. Phys.*, *20*(8), 1309–1314.
- Barnes, P. R. F., and E. W. Wolff (2004), Distribution of impurities in cold glacial ice, *J. Glaciol.*, *50*, 311–324.
- Barnes, P. R. F., E. W. Wolff, R. Mulvaney, R. Udisti, E. Castellano, R. Röthlisberger, and J.-P. Steffensen (2002), Effect of density on electrical conductivity of chemically laden polar ice, *J. Geophys. Res.*, *107*(B2), 2029, doi:10.1029/2000JB000080.
- Barrella, T., S. Barwick, and D. Saltzberg (2011), Ross Ice Shelf (Antarctica) in situ radio-frequency attenuation, *J. Glaciol.*, *57*(201), 61–66.
- Camplin, G. C., J. W. Glen, and J. G. Paren (1978), Theoretical models for interpreting the electrical behaviour of HF-doped ice, *J. Glaciol.*, *21*(85), 123–141.
- Cole-Dai, J. (2004), Sulfate-based volcanic record from South Pole ice cores, National Snow and Ice Data Center, Boulder, CO, <http://nsidc.org/data/nsidc-0215.html>.
- Dowdeswell, J. A., and S. Evans (2004), Investigations of the form and flow of ice sheets and glacier using radio-echo sounding, *Rep. Prog. Phys.*, *67*(10), 1821–1861, doi:10.1088/0034-4885/67/10/R03.
- Fitzgerald, W. J., and J. G. Paren (1975), The dielectric properties of Antarctic ice, *J. Glaciol.*, *15*, 39–48.
- Fujita, S. et al. (2002), Linear and non-linear relations between the high-frequency-limit conductivity, AC-ECM signals and ECM signals of Dome F Antarctic ice core from a laboratory experiment, *Ann. Glaciol.*, *35*, 321–328.
- Fukazawa, H., K. Sugiyama, S. Mae, S. Narita, and T. Hondoh (1998), Acid ions at triple junction of Antarctic ice observed by Raman scattering, *Geophys. Res. Lett.*, *25*(15), 2845–2848.
- Glen, J. W., D. R. Homer, and J. G. Paren (1977), Water at grain boundaries: Its role in the purification of temperate glacier ice, in *Isotopes and Impurities in Snow and Ice*, pp. 263–271, IAHS-AISH Publications, Wallingford, U. K.
- Grimm, R. E., D. E. Stillman, S. F. Dec, and M. Bullock (2008), A. Low-frequency electrical properties of polycrystalline saline ice and salt hydrates, *J. Phys. Chem. B*, *112*(48), 15,382–15,390, doi:10.1021/jp8055366.
- Gross, G. W., P. M. Wong, and K. Humes (1977), Concentration dependent solute redistribution at the ice-water phase boundary. III. Spontaneous convection. Chloride solutions, *J. Chem. Phys.*, *67*(11), 5264–5274.
- Hammer, C. U. (1980), Acidity of polar ice cores in relation to absolute dating, past volcanism, and radio-echoes, *J. Glaciol.*, *25*(93), 359–372.
- Hammer, C. U. (1983), Initial direct current in the buildup of space charges and the acidity of ice cores, *J. Phys. Chem.*, *87*, 4099–4103.
- Jaccard, C. (1959), Thermodynamics of irreversible processes applied to ice, *Phys. Kondens. Mater.*, *3*, 99–118.
- Jacobel, R. W., B. C. Welch, D. Osterhouse, R. Pettersson, and J. A. MacGregor (2009), Spatial variation of radar-derived basal conditions on Kamb Ice Stream, West Antarctica, *Ann. Glaciol.*, *50*(51), 10–16.
- Jacobel, R. W., K. E. Lapo, J. R. Stamp, B. W. Youngblood, B. C. Welch, and J. L. Bamber (2010), A comparison of basal reflectivity and ice velocity in East Antarctica, *Cyrosphere*, *4*, 447–452, doi:10.5194/tc-4-447-2010.
- Johari, G. P., and E. Whalley (1981), The dielectric properties of ice Ih in the range 272–133 K, *J. Phys. Chem.*, *75*(3), 1333–1340.
- Kawada, S. (1978), Dielectric anisotropy in ice Ih, *J. Phys. Soc. Japan*, *44*(6), 1881–1886.
- Keller, B. V. (1982), Electrical properties of rocks and minerals, in *Handbook of Physical Properties of Rocks*, vol. 1, edited by R. S. Carmichael, pp. 217–224, CRC Press, Boca Raton, FL.
- Keller, G.V., and F. C. Frischknecht (1960), Electrical resistivity studies on the Athabasca glacier, Alberta, Canada. *J. Res. NBS*, *64D*(5), 439–448.
- Kopp, M. (1962), Conductivité électrique de la neige, au courant continu, *J. Math. Phys. Appl.*, *13*, 431–441.
- Kulassa, B. (2007), A critical review of the low-frequency electrical properties of ice sheets and glaciers, *J. Environ. Eng. Geophys.*, *12*(1), 23–36.
- Legrand, M., and P. Mayewski (1997), Glaciochemistry of polar ice cores: A review, *Rev. Geophys.*, *35*(3), 219–243.
- Lide, D. R. (2008), *Handbook of Chemistry and Physics*, 88th ed., CRC Press, Boca Raton, FL.
- MacGregor, J. A., D. P. Winebrenner, H. B. Conway, K. Matsuoka, P. A. Mayewski, and G. D. Clow (2007), Modeling englacial radar attenuation at Siple Dome, West Antarctica, using ice chemistry and temperature data, *J. Geophys. Res.*, *112*, F03008, doi:10.1029/2006JF000717.
- MacGregor, J. A., S. Anandakrishnan, G. A. Catania, and D. P. Winebrenner (2011), The grounding zone of the Ross Ice Shelf, West Antarctica, from ice-penetrating radar, *J. Glaciol.*, *57*(205), 917–928.
- MacGregor, J. A., K. Matsuoka, E. D. Waddington, D. P. Winebrenner, and F. Pattyn (2012), Spatial variation of englacial radar attenuation: Modeling approach and application to the Vostok flowline, *J. Geophys. Res.*, *117*, F03022, doi:10.1029/2010JF002327.
- Maeno, N. (1978), The electrical behaviors of Antarctic ice drilled at Mizuho Station, East Antarctica, *Mem. Natl. Inst. Polar Res.*, *10*, 77–94.
- Matsuoka, K., F. Pattyn, D. Callens, and H. Conway (2012), Radar characterization of the basal interface across the grounding zone of an ice-rise promontory in East Antarctica, *Ann. Glaciol.*, *53*(60), 29–34, doi:10.3189/2012AoG60A106.
- Mayewski, P. A., et al. (1995a), An ice-core based, late Holocene history for the Transantarctic Mountains, Antarctica, *Antarct. Res. Ser.*, *67*, 33–45.
- Mayewski, P. A., et al. (1995b), Climate change during the last deglaciation in Antarctica, *Science*, *272*(5268), 1636–1638.
- Moore, J. C., E. W. Wolff, H. B. Clausen, and C. U. Hammer (1992a), The chemical basis for the electrical stratigraphy of ice, *J. Geophys. Res.*, *97* (B2), 1887–1896.
- Moore, J., J. Paren, and H. Oerter (1992b), Sea salt dependent electrical conduction in polar ice, *J. Geophys. Res.*, *97*(B13), 19,803–19,812.
- Moore, J. C., E. W. Wolff, H. B. Clausen, C. U. Hammer, M. Legrand, and K. Fuhrer (1994a), Electrical response of the Summit-Greenland ice core to ammonium, sulphuric acid, and hydrochloric acid, *Geophys. Res. Lett.*, *21*(7), 565–568.
- Moore, J. C., A. P. Reid, and J. Kipfstuhl (1994b), Microstructure and electrical properties of marine and its relationship to meteoric ice and sea ice, *J. Geophys. Res.*, *99*(C3), 5171–5180.
- Mulvaney, R., E. W. Wolff, and K. Oates (1988), Sulphuric acid at grain boundaries in Antarctic ice, *Nature*, *331*(6153), 247–249.
- Nye, J. F., and F. C. Frank (1973), Hydrology of the intergranular veins in a temperate glacier, in *Hydrology of Glaciers*, pp. 157–161, IAHS-AISH Publications, Wallingford, U. K.
- Obbard, R., and I. Baker (2007), The microstructure of meteoric ice from Vostok, Antarctica, *J. Glaciol.*, *53*(180), 41–62.
- Paren, J. G. (1973), The electrical behaviour of polar glaciers, in *Physics and Chemistry of Ice*, edited by E. Whalley, S. J. Jones, and L. W. Gold, pp. 262–267, Royal Society of Canada, Ottawa.
- Petit, J. R., et al. (1999), Climate and atmospheric history of the past 420,000 years from the Vostok ice core, Antarctica, *Nature*, *399*(6735), 429–436.
- Petrenko, V. F., and R. W. Whitworth (1999), *Physics of Ice*, 1st ed., Oxford Univ. Press, Oxford, U. K.
- Reynolds, J. M. (1985), Dielectric behaviour of firm and ice from the Antarctic Peninsula, Antarctica, *J. Glaciol.*, *31*(109), 253–262.
- Reynolds, J. M., and J. G. Paren (1980), Recrystallisation and the electrical behaviour of glacier ice, *Nature*, *283*(5742), 63–64.
- Reynolds, J. M., and J. G. Paren (1984), Electrical resistivity of ice from the Antarctic Peninsula, Antarctica, *J. Glaciol.*, *30*(106), 289–295.
- Shabtaie, S., and C. R. Bentley (1995), Electrical resistivity sounding of the East Antarctic ice sheet, *J. Geophys. Res.*, *100*(B2), 1933–1954.
- Souchez, R., et al. (2002), Highly deformed basal ice in the Vostok ice core, Antarctica, *Geophys. Res. Lett.*, *29*(7), 1136, doi:10.1029/2001GL014192.
- Srikanta Dani, K. G., H. M. Mander, E. W. Wolff, and J. L. Wadham (2012), Modelling the liquid-water vein system with polar ice sheets as a potential microbial habitat, *Earth Planet Sci. Lett.*, *333–334*, 238–249, doi:10.1016/j.epsl.2012.04.009.
- Stillman, D. E., R. E. Grimm, and S. F. Dec (2010), Low-frequency electrical properties of ice–silicate mixtures, *J. Phys. Chem. B*, *114*(18), 6065–6073, doi:10.1021/jp9070778.
- Stillman, D. E., J. A. MacGregor, and R. E. Grimm (2013), Electrical response of ammonium-rich water ice, *Ann. Glaciol.*, *64*(54), 6, doi:10.3189/2013AoG64A204.
- Takei, I., and N. Maeno (1987), Electrical characteristics of point defects in HCl-doped ice, *J. Phys.*, *48*(C1), 121–126.
- Taylor, K. C., R. B. Alley, J. Fiacco, P. Grootes, G. Lamorey, P. Mayewski, and M. J. Spencer (1992), Ice-core dating and chemistry by direct-current electrical conductivity, *J. Glaciol.*, *38*(130), 325–332.
- Taylor, K. C., et al. (1993), The ‘flickering switch’ of late Pleistocene climate change, *Nature*, *361*, 432–436.
- Taylor, K. C., R. B. Alley, G. W. Lamorey, and P. Mayewski (1997), Electrical measurements on the Greenland Ice Sheet Project 2 Core, *J. Geophys. Res.*, *102*(C12), 26,511–26,517.

- Torres-Verdin, C., F. O. Alpak, and T. M. Habashy (2006), Petrophysical inversion of borehole array-induction logs: Part II – Field data examples, *Geophysics*, *71*(5), 261–268, doi:10.1190/1.2335633.
- Wolff, E. (2000), Electrical stratigraphy of polar ice cores: Principles, methods, and findings, in *Physics of Ice Core Records*, edited by T. Hondoh, pp. 155–171, Hokkaido Univ. Press, Sapporo, Japan.
- Wolff, E. W., and J. G. Paren (1984), A two-phase model of electrical conduction in polar ice sheets, *J. Geophys. Res.*, *89*(B11), 9433–9438.
- Wolff, E. W., J. C. Moore, H. B. Clausen, C. U. Hammer, J. Kipfstuhl, and K. Fuhrer (1995), Long-term changes in the acid and salt concentrations of the Greenland Ice Core Project ice core from electrical stratigraphy, *J. Geophys. Res.*, *100*(D8), 16, 249–16, 263.
- Wolff, E. W., W. D. Miners, J. C. Moore, and J. G. Paren (1997), Factors controlling the electrical conductivity of ice from the polar regions—A summary, *J. Phys. Chem. B*, *101*(32), 6090–6094.
- Wolff, E. W., J. S. Hall, R. Mulvaney, E. C. Pasteur, D. Wagenbach, and M. Legrand (1998), Relationship between chemistry of air, fresh snow and firn cores for aerosol species in coastal Antarctica, *J. Geophys. Res.*, *103*(D9), 11,057–11,070.
- Yang, Q., P. A. Mayewski, M. Twickler, and S. Whitlow (1997), Major features of glaciochemistry over the last 110,000 years in the Greenland Ice Sheet Project 2 ice core, *J. Geophys. Res.*, *102*(C12), 23,289–23,299.